2022

Fabrication and Characterization of Novel AgNPs Functionalized with Chlorothymol (C@AgNPs)

Lirim Sopaj
Wright State University

FABRICATION AND CHARACTERIZATION OF NOVEL AgNPs FUNCTIONALIZED WITH CHLOROTHYMOL (C@AgNPs)

A thesis submitted in partial fulfillment of the

requirements for the degree of

Master of Science

by

LIRIM SOPAJ

Bach., University of Prishtina, Kosovo, 2018

2022

Wright State University

WRIGHT STATE UNIVERSITY
GRADUATE SCHOOL

April 20, 2022

I HEREBY RECOMMEND THAT THE THESIS PREPARED UNDER MY SUPERVISION BY Lirim Sopaj ENTITLED Fabrication and characterization of novel AgNPs functionalized with chlorothymol (C@AgNPs) BE ACCEPTED IN PARTIAL FULFILLMENT OF THE REQUIREMENTS FOR THE DEGREE OF Master of Science.

_____
Ioana E. Pavel, Ph.D.
Thesis Director

_____
Audrey McGowin, Ph.D.
Chair, Department of Chemistry

Committee on Final Examination:

_____
Ioana E. Pavel, Ph.D.

_____
David A. Dolson, Ph.D.

_____
Steven R. Higgins, Ph.D.

_____
Travis B. Clark, Ph.D.

_____
Barry Milligan, Ph.D.
Vice Provost for Academic Affairs
Dean of the Graduate School

ABSTRACT

Sopaj, Lirim M.S., Department of Chemistry, Wright State University, 2022. Fabrication and Characterization of Novel AgNPs Functionalized with Chlorothymol (C@AgNPs)

In this study, novel silver nanoparticles (AgNPs) were successfully synthesized and functionalized with an antibacterial agent, namely chlorothymol (denoted C@AgNPs). The resulting colloid (C@AgNPs) was purified by two comparative methods: ultrafiltration and ultracentrifugation. Ultrafiltration proved to be more efficient in purifying and size selecting (10 kD filter) and concentrating the C@AgNPs than ultracentrifugation. The physicochemical properties of the filtered C@AgNPs were then characterized by UV-Vis absorption spectroscopy, inductively coupled plasma optical emission spectroscopy (ICP-OES), Raman spectroscopy, Cytoviva hyperspectral imaging, and Scanning electron microscopy. These measurements confirmed the functionalization of the core AgNPs with chlorothymol and suggest the proposed mechanism of C@AgNP formation through a coordinate covalent bond between the oxygen atom of chlorothymol and the Ag atoms at the nano surface.

Table of Contents

List of Figures

List of Tables

Acknowledgments

I would first like to thank Dr. Ioana E. Pavel for accepting me into her research group and guiding me through this challenging project. She has been very kind and always encouraged me to go beyond my comfort zone. Her advice has been much appreciated.

I would also like to thank Dr. Dolson, Dr. Higgins, and Dr. Clark, for guiding me through the graduate studies and their valuable input on this research project. I am grateful to Dr. Kanel who helped me collecting the SEM/EDX data. His willingness to help me was a very kind and generous gesture from his part and I appreciate him for that. A huge thank to Joseph Minneman, the undergraduate student who helped me with the silver nanoparticle synthesis set up and filtration process. I want to thank Praveen, Nicole, Harsimran, Avianna, and Jordan, graduate students in our research group for their continuous support, feedback, and kind attitude towards me. Also, my sincere thanks to the previous student in our research group, Kristina Steingass, who volunteered to train me on the silver nanoparticle synthesis via modified Creighton method and purifying techniques our lab is currently using.

Specials thanks to the Chemistry Department at WSU for the financial support and the opportunity to further develop my passion for chemistry.

I am also grateful to my family and friends who supported me during these challenging times.

Introduction

Silver has been known for its antibacterial activity for more than 2,000 years and is incorporated as nano silver into numerous consumer products due to its antimicrobial properties.[1] Examples of such products include dental resin composites, coating of medical devices, air sanitizers spray, pillows, socks, wet wipes, detergents, soaps, shampoos, and toothpastes.[1]

Silver nanoparticles (AgNPs) range between 1-100 nm in size and their antibacterial activity was related to cell membrane damage and the generation of reactive oxygen species (ROS).[2, 3] Cell membrane damage was associated with the AgNPs' interaction with thiol groups residing in the cell wall, which lead to the inactivation of the membrane-bound enzymes and proteins.[4] In addition, the presence of the AgNPs at the cell membrane results in an increase of the trans/cis ratio of unsaturated fatty acids, which causes a permanent loss of membrane integrity and increased permeability.[4] Generation of ROS species (e.g., hydroxyl radicals and superoxide radicals) is associated with the oxidation of the double bonds of fatty acids. Silver (soft acid) can also damage the DNA of a living cell as the result of its direct interaction with phosphorous and sulfur (soft bases), which are major components of the cell DNA.[5] Increasing the size of AgNPs to sub ~10 nm has been shown to increase their antibacterial activity.[2, 4] This is due to the increase of the surface area to volume (SA/V) ratio with the decrease in the particle size.[6]

In addition, small AgNPs (~5 nm) are accompanied by an excess energy at the surface because of the sharp increase in their band gap energy,[3] which causes crystallographic changes such as rearrangements of the surface atoms and enhances their direct interaction with bacteria cells.[3, 7, 8]

Functionalization of NPs enhances or improves specific properties by introducing chemicals or biomolecules to the surface via covalent or non-covalent binding to the NP surface.[9] Functionalization affects NP characteristics such as size, charge, surface chemistry, hydrophilicity, and hydrophobicity, which in turn can impact their solubility, biocompatibility, and biodistribution.[7, 9] For example, functionalization of AgNPs with thymol (Figure 1) was observed to increase the antibacterial properties of AgNPs.[10] This synthesis was achieved by first encapsulating core AgNPs into a chitosan layer, a natural polycationic linear polysaccharide,[11] which then served as an anchoring point for thymol.[10] These AgNPs functionalized with thymol had a relatively small mean diameter (28.98 nm), good stability in water, but very limited loading efficiency (3.5 ± 1 %).[10]

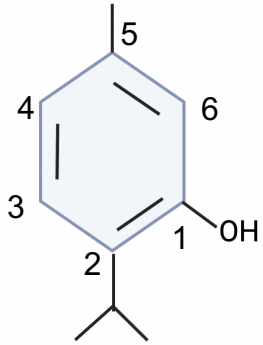

Figure 1. Chemical structure of thymol (made in ©BioRender-biorender.com).

Thymol (2-isopropyl-5-methylphenol) is a naturally occurring monoterpenoid phenolic organic compound, which is present in the essential oils extracted from the thyme plant (Figure 1).[12] At neutral pH, it is poorly soluble in water but soluble in organic solvents such as alcohols.[13] Thymol is an U.S. Food and Drug Administration (FDA)-approved food additive and is Generally Recognized As a Safe (GRAS) product.[14] A substance can be classified as GRAS by the U.S. FDA, only if there is enough available data about the safety of its use. This means that the scientific studies must conclude with a reasonable certainty that the substance is not harmful for the intended use as direct food additive.[15] Due to its antioxidant, antimicrobial, antifungal, and anti-inflammatory properties, thymol has been used as an alternative treatment for cavities and dental plaques.[12]

Chlorothymol is a halogenated derivative of thymol (Figure 2), which is synthetically manufactured,[16] but relatively inexpensive (less than $2 per gram).[17] Previous studies have evaluated the antimicrobial, antifungal, antimalarial, and antiseizure properties of chlorthymol.[17,18] However, chlorothymol is not established yet as a Generally Recognized as Safe (GRAS) product.[19] As of May 7th, 1991, chlorothymol was U.S. FDA-approved as a topical antifungal drug for diaper rash products [20] and as a denaturant for alcoholic solutions of antiseptics, perfumes, shampoos, soap preparations, disinfectants, insecticides, fungicides, sterilizing, and preserving agents.[19]

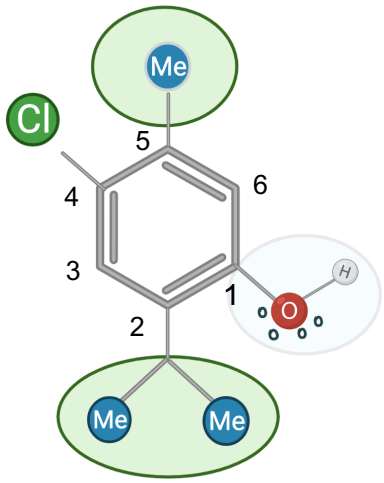

Figure 2. Chemical structure of chlorothymol with numbered carbon atoms on the aromatic ring (made in ©BioRender- biorender.com).

Chlorothymol was found to exhibit enhanced antibacterial properties when compared to thymol due to the presence of the chlorine atom at the position #4 in the phenol ring.[16] The antibacterial properties of different halogenated derivatives of thymol, which introduce a chlorine atom at positions #3 and/or #4, or a bromine atom at position #6, were also investigated.[16] Chlorothymol having the chlorine atom at the position #4 had the highest antibacterial activity, while all other positions resulted in the complete loss of antibacterial activity.[16] However, no mechanistic explanation was provided for the enhanced antibacterial activity of chlorothymol when compared to thymol alone or other substituted thymol structures (Cl, Br, and I).[16] To the best of our knowledge, this is the first study focusing on the functionalization of AgNPs with chlorothymol. Once fabricated, these AgNPs

were purified by two comparative methods (ultracentrifugation and ultrafiltration) and were characterized by UV-Vis absorption spectroscopy, inductively coupled plasma optical emission spectroscopy (ICP-OES), Raman spectroscopy, Cytoviva enhanced dark imaging, and scanning electron microscopy (SEM).

UV-Vis absorption spectroscopy was selected to confirm the formation of AgNPs through the surface plasmon resonance (SPR) effect and stability overtime. UV-Vis absorption spectroscopy measures the amount of light (UV or visible light) absorbed or transmitted through a sample when compared to a reference sample.[21] Metal nanoparticles such as silver or gold NPs, tend to strongly interact with specific wavelengths of the light, thus providing unique optical properties. Exposure of metal nanoparticles with free conduction electrons on their surface atoms to light causes their collective oscillation.[22] This polarization of the free conduction electrons on the NP surface and creation of an internal *E* field is known as the surface plasmon resonance (SPR) effect.[22] Silver is known to have the strongest plasmonic interaction with light [23] and its SPR lies in the UV region.[24] The SPR of silver NPs was observed to shift to shorter wavelengths, when the size of the NPs decreased.[24] In a typical UV-Vis measurement, the photons that are not absorbed or scattered by the sample are measured. This is known as the transmittance of a sample expressed as I/I_0, where I is the intensity of photons that have passed through the sample, and I_0 the incident photons. However, it is very common to represent the UV-Vis measurement as

Absorbance (*A*) where the relationship between the absorbance and transmittance is $A = -\log_{10}(T)$.[25] In the near infrared region (IR), where most NP samples do not absorb, the transmittance is almost 100 %. In the ultraviolet region (UV) where the samples absorb, the transmittance is in indirect proportion with concentration: the less concentrated the sample, the greater the transmittance value.[25] The UV-Vis spectroscopy also provides information about the stability of the NP suspensions. If NP-aggregates are present in the sample, the optical properties of the NPs change, and this change is accompanied by a shift of the characteristic SPR peaks to lower energy. NP-aggregation may also cause a peak broadening or the appearance of secondary peaks at longer wavelengths.[25] However, UV-Vis spectroscopy provides limited qualitative information (it is able to identify only the compounds containing chromophore groups in their structure) and it is not suitable for multicomponent analysis.[26]

Inductively coupled plasma-optical emission spectroscopy (ICP-OES), a well-established analytical technique,[27] was selected for the quantification of Ag down to low parts per billion (ppb) level. ICP-OES is commonly utilized for the detection of metal ions such Ag and Pb in wastewater or rice samples.[27] In this study, ICP-OES facilitated the determination of the total Ag concentration before and after the NP functionalization with chlorothymol. To achieve this, calibrating solutions with known concentrations of the analyte elements and the sample solutions were introduced into the plasma and measured at specific light wavelength of the analyte line (e.g., 328.068 and

338.289 nm for Ag).[2, 28] A calibration curve of the Ag calibration solutions using the corresponding emission intensities was then prepared and utilized for the estimation of the total Ag concentration in the sample, through interpolation.[28] ICP-OES advantages include rapid and simultaneous multielement analysis, low detection limits (ppb), high precision (0.5 %- 5%), small interference from the matrix, and measurement of samples in all physical states. ICP-OES disadvantages consist of potential spectral interferences, difficulty analyzing solids without dissolution, and /or insufficient sample aspiration.[27]

Raman spectroscopy was employed to characterize the chemical functionalization of AgNP surface with chlorothymol. Changes in the Raman spectral profile of the colloidal AgNPs after exposure to chlorothymol such as significant differences in peak intensity, peak shifts, or appearance of new peaks are indicative of a possible chemical interaction of AgNPs with chlorothymol. Raman spectroscopy is a non-destructive and non-invasive molecular fingerprinting technique, which can provide real-time information about the AgNP-chlorothymol interaction at the molecular level.[29] The Raman peaks in the spectrum represent the “molecular fingerprint” of the sample, which facilitate the identification of Raman active chemical bonds (e.g., molecules exhibiting change in the polarizability tensor).[29] Raman spectroscopy utilizes the inelastic scattering properties of the sample, and it is based on Raman effect (the frequency of the scattered radiation is different from the frequency of the incident monochromatic radiation).[30] Briefly, the

scattered radiation is observed after the interaction of sample with monochromatic laser beam. This scattered radiation has a frequency that is different from the incident radiation and is utilized to construct the Raman spectrum. The Raman spectrum is plotted as intensity-versus-wavelength shift, typically in the 100-4000 cm^{-1} range. [30] Disadvantages include limited detection capabilities at low analyte concentrations (i.e., only one out of ~10^6 incident photons will inelastic scattering effects) and potential fluorescence interferences.[31]

CytoViva hyperspectral imaging was utilized to study interaction of AgNPs with chlorothymol. More specifically, it helped monitor the size distribution of AgNPs before and after functionalization with chlorothymol molecules. In CytoViva, the sample is illuminated with light and unique profiles of scattered light are generated as the interaction between light and sample occurs. These unique profiles are represented as spectral signatures and are characteristic for each target. The generated images exhibit enhanced contrast signal to noise ratio due to dark field illumination. Dark field illumination is achieved by a special size disc that blocks the illumination so that only the inclined rays interact with the sample.[32]

The incoming scattered light from the sample appears as bright spots while all the other objects with similar but not the same refractive indexes are considered as the background.[32] CytoViva enhanced darkfield imaging offers an improved signal to noise ratio (up to ten times) when compared to

standard darkfield imaging and facilitates the visualization of NPs as small as 10 nm in solutions or cells. It is often used to study the interaction of NPs with cells and the effect of nanoparticles on the cells being studied.[32, 33] Furthermore, fast, and rapid measurements can be completed with minimal sample preparation.[33] This is a new technology with promising applications in nanoscience and nanotechnology. However, CytoViva hyperspectral libraries are usually not available for the discrimination of nanomaterials in translucent matrices such as cell and tissues.[34]

In this project, scanning electron microscopy (SEM) was employed for imaging AgNPs (size and size distribution) and for conducting a chemical composition analysis of AgNPs after functionalization with chlorothymol. SEM is an imaging technique that uses a high energy beam of electrons to gain information about the surface of solid samples. Briefly, it can provide information about the size, shape, crystalline structure, and surface morphology of both micro and nano scale samples. The SEM images can be analyzed using specialized software (e.g., ImageJ) to create size histograms with detailed information about the size distribution and the aggregation of AgNPs.[35] Briefly, a high energy beam of electrons interacts with the sample and different type of signals are observed: secondary electrons, backscattered electrons, diffracted backscattered electrons, and photons (X-ray). Secondary and backscattered electrons produce SEM images, while diffracted backscattered electrons may be used to determine the crystalline structure. X-rays may be used to determine elemental composition as the

result of the interaction (collision) between the incident electrons with the electrons residing in specific orbitals of atoms of the sample. The excited electrons release X-rays with a specific wavelength, when returning to the lower energy state.[36]

Each element produces characteristic X-rays, thus making it possible to precisely differentiate multiple elements within a sample.[36]

Main Goal and Specific Aims

Main Goal: The main objective of this study to fabricate and characterize novel silver nanoparticles (AgNPs) functionalized with chlorothymol.

Specific Aim 1: To synthesize, size select, concentrate, and purify core AgNPs and AgNPs functionalized with chlorothymol by two comparative methods, namely ultracentrifugation and ultrafiltration.

Specific Aim 2: To characterize the physicochemical properties of AgNPs using UV-vis absorption spectroscopy, inductively coupled plasma-optical emission spectroscopy (ICP-OES), Raman spectroscopy, CytoViva hyperspectral imaging, and scanning electron microscopy (SEM)

Material and Methods

Materials

Silver nitrate (>99%, $AgNO_3$), sodium borohydride (99 %, $NaBH_4$), and ethanol (99%, CH_3CH_2OH) were purchased from Acros Organics. 4-Chlorothymol (99%) was obtained from Sigma Aldrich. All chemicals in this study were used without further modification. High quality water (>18 MΩ cm, HQ water) was utilized as solvent for the preparation of the sodium borohydride and silver nitrate reagent solutions. OPTIMA grade nitric acid (HNO_3) was obtained for the trace metal analysis by ICP-OES.

Synthesis of core silver nanoparticles (AgNPs)

Core AgNPs (3.8 L) were synthesized following the Creighton method modified by our lab, through the reduction of Ag^+ ions from $AgNO_3$ to silver zero in an ice-cold, aqueous solution of $NaBH_4$.[37] Briefly, a 2 mM of $NaBH_4$ solution was prepared in 150 mL of cold water (4 °C) and 25 mL of 1.0 mM $AgNO_3$ solution was then added dropwise to this solution. The solution was continuously stirred with a magnetic bar (350 rpm) for 1 hour. The change in color from colorless to light yellow indicated the formation of the core, colloidal AgNPs. The core AgNPs were stabilized for another 1 hour under constant stirring and then stored at 4 °C for further characterization. The desired volume (3.8 L) was achieved in a batch-wise process utilizing the modified Creighton method.[37, 38]

The resulting colloid of AgNPs was characterized via UV-Vis absorption spectroscopy, Raman spectroscopy, CytoViva hyperspectral imaging, and scanning electron microscopy (SEM).

Functionalization of silver nanoparticles with chlorothymol (C@AgNPs)

Equal volumes (10 mL) of core AgNPs suspensions and chlorothymol (0.5 g dissolved in 100 mL of ethanol, 99%) were mixed with continuous stirring (350 rpm), for 5 minutes (Figure 3). The resulting suspension was mixed in a water bath sonicator (Mettler Electronics corp.), at 35 °C, for 2 hours. The change of color to a muddy brown confirmed the loading of chlorothymol to the surface of core AgNPs. Two comparative methods were utilized for the purification of the C@AgNPs: ultracentrifugation and ultrafiltration.

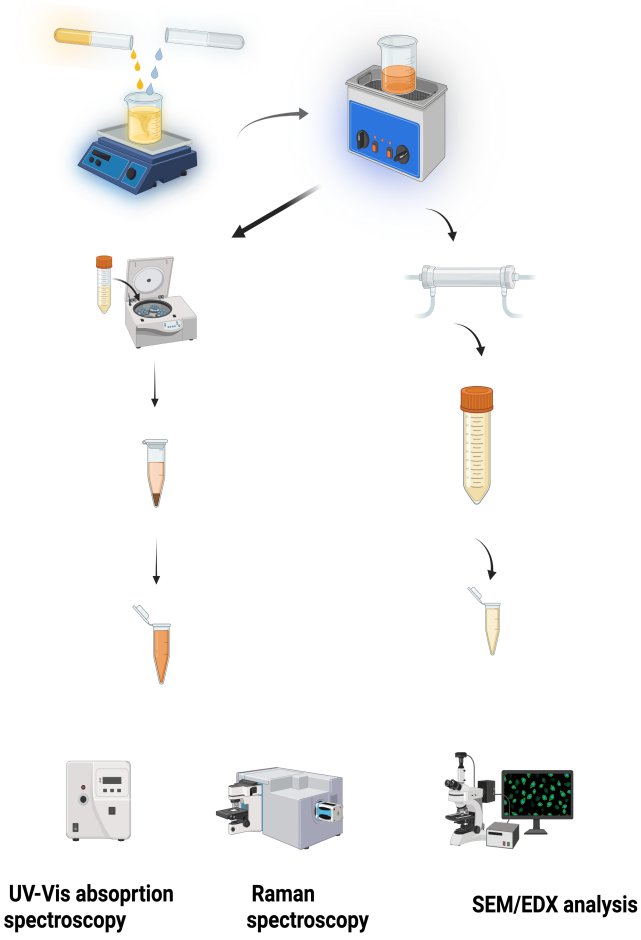

Figure 3. Schematic of the synthesis, functionalization with chlorothymol, purification, and physicochemical characterization processes of C@AgNPs (made in ©BioRender -biorender.com).

Ultrafiltration of core AgNPs and AgNPs functionalized with chlorothymol (C@AgNPs)

First, AgNPs suspensions were filtered by the automated ultrafiltration using a 500 kD and a 10 kD mPES filter (Spectrum Labs, Inc.) in a tangential flow filtration (TFF) system (Spectrum Labs, Inc) as described below. The two-step TFF procedure was employed to purify, size-select, and concentrate the original, core AgNPs and C@AgNPs. Briefly, the colloidal suspension was aspirated and subsequently pushed by a peristaltic pump (KrosFlo® KR2i, 250 mL min^{-1}) through two hollow fiber membrane filters of 500 kD and 10 kD. Solids (i.e., core AgNPs and C@AgNPs) larger than the pore size of the filter were collected in a retentate flask and stored for further characterization, while those smaller than the pore size were denoted as permeate. The permeate was mainly composed of solvent (water molecules), small core AgNPs, and excess reagents (free chlorothymol molecules) (Figure 4).[39]

In this study, 3.8 L of colloidal AgNPs were first filtered using a 500 kD modified polyether sulfone (mPES) hollow-fiber filter membrane (Spectrum Labs, Inc., 20 cm^2) (Figure 4). This yielded a concentrated retentate (80 mL) and a filtrate (3.65 L). The filtrate (3.65 L) was further processed using a 10 kD modified polyether sulfone (mPES, 20 cm^2) hollow-fiber filter membrane (Spectrum Labs, Inc.). This resulted into 85 mL of ultraconcentrated retentate,

which was stored at 4 °C and used within 2 weeks. After functionalization, 500 mL of C@AgNPs were first filtered through a 0.45 µm nitrocellulose membrane filter (Fisher Scientific). The filtrate (490 mL) was collected and processed using a 10 kD mPES filter (Spectrum Labs, Inc.) down to a ~ 50 mL of final 10 kD retentate. The final 10 kD suspension containing AgNPs functionalized with chlorothymol, C@AgNPs, were stored at 4 °C until characterization.

Ultracentrifugation of AgNPs functionalized with chlorothymol (C@AgNPs)

Ultracentrifugation (Mettler Electronics Corp.) was performed at 13,000 rpm (21,161 G) to separate the pellet containing the functionalized AgNPs (C@AgNPs) from the supernatant having free chlorothymol molecules and smaller particulates. The pellet was resuspended in 2.5 mL deionized water, while the supernatant was saved for later analysis.

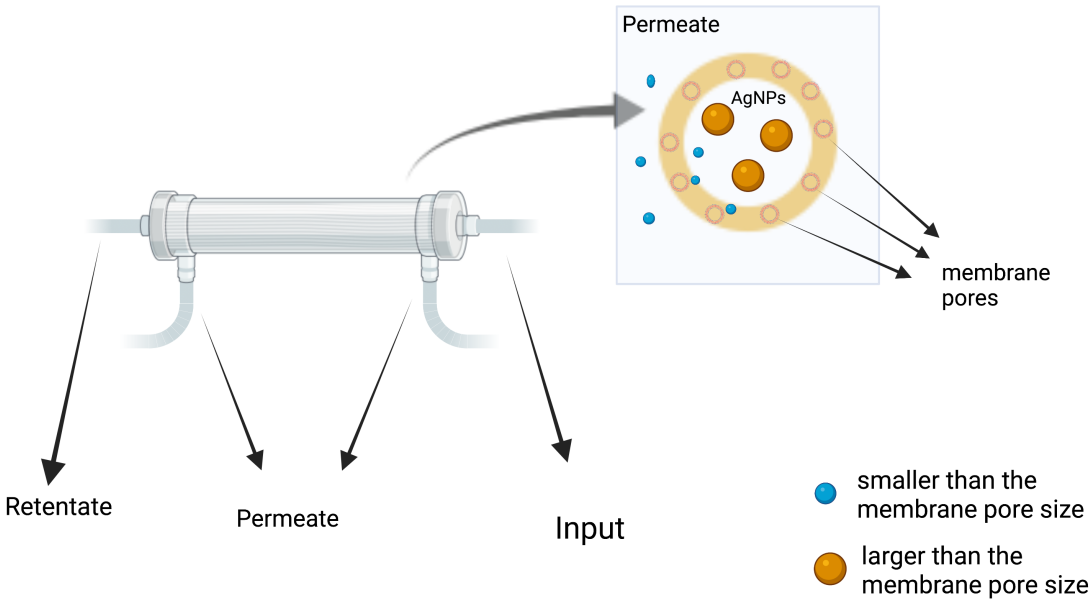

Figure 4. Schematic of the Tangential Flow Filtration (TFF) working principle using hollow membrane fibers of a certain pore size. The retentate contains silver nanoparticles (AgNPs) that are larger than the pore size, while the permeate contain AgNPs that are smaller than the pore size (made in ©BioRender -biorender.com).

UV-Vis absorption spectroscopy of core AgNPs and C@AgNPs

Small aliquots **(**~1 mL) of the ultrafiltration and ultracentrifugation concentrates of AgNPs and C@AgNPs were diluted with 2.5 mL of HQ water and placed in a quartz cuvette (1 cm path length). UV-Vis absorption spectra were recorded using a Varian Cary Bio 50 spectrophotometer, at a fast scan rate of 4800 nm min^{-1}, from 200 nm to 800 nm. Spectral resolution was 1 nm. Origin 8 pro software was utilized for data processing.[2, 38]

Raman spectroscopy of core AgNPs and ultrafiltered C@AgNPs

Small aliquots (~1 mL) of core AgNPs and ultrafiltered C@AgNPs were transferred to 2 mL quartz cuvettes and diluted with HQ water to the top of the cuvette. Their respective Raman spectra were collected using a LabRam HR-800 (Horiba Jobin Yvon, Inc.) system equipped with an internal laser beam (632.8 nm, 15 mW output) of a spot diameter of ~1 μm. The BX41 microscope coupled to an Olympus objective (100x) and a confocal hole of 300 μm were employed. A thermoelectrically cooled CCD detector (1024 x 256 pixels) was employed for the data collection in the 100-400 cm^{-1} spectral range, at 3 cycles, with acquisition times of 30 s. Spectral resolution was ~1 cm^{-1}. The spectra were collected in LabSpec v.5 and processed in Origin 8 pro software.[2, 38]

SEM analysis on core AgNPs and ultrafiltered C@AgNPs

Approximately 1 mL of core AgNPs, ultracentrifuged C@AgNPs, and ultrafiltered C@AgNPs were deposited through drop casting onto stem stubs. The samples were then allowed to dry for 4 days, at room temperature, prior to performing the SEM analysis. The microstructure of the components was examined using an Apreo FESEM, at an operating voltage of 15 kV and a working distance of 10 nm.

SEM images, electron dispersive X-ray spectroscopy (EDS), and electron backscatter diffraction (EBSD) data were collected from specimens with the help of a FEI Apreo scanning electron microscope (SEM) equipped with Oxford N-Max EDX and Oxford Symmetry EBSD detectors.

Inductively coupled plasma-optical emission spectroscopy (ICP-OES) of core AgNPs and ultrafiltered C@AgNPs

ICP-OES uses a partially ionized argon gas produced in a quartz torch, where the sample is introduced into the center of the plasma as aerosols. The analyte signal or the emission intensity depends on the number of ions (analyte ions or atoms) that are excited from the sample.[28]

Core AgNPs and ultrafiltered C@AgNPs samples (10 µL each) were cold digested by mixing with 3.0 mL of OPTIMA grade HNO_3, for 15 minutes, at room temperature. Hot digestion was followed by heating at 275 °C, until the volume was reduced to ~10 µL. The samples were then diluted in 10 mL volumetric flasks with 286 µL of OPTIMA grade HNO_3 and HQ water to a final 2% HNO_3.

A Varian 710 ICP-OES instrument equipped with a SPS 3 autosampler was utilized for the sample analysis at a pump rate of 2 mL min^{-1}. A sample uptake of 40 s and a triplicate read time of 15 s were applied. Thirteen standards (0, 25, 50, 75, 100, 125, 150, 200, 300, 400, 500, 600, and 700 µg L^{-1}) were prepared through dilution in 2% OPTIMA grade HNO_3, from a Ag^+ stock (1000 mg L^{-1}, SPEX CertiPrep) and were utilized in the creation of an external calibration curve. The analysis was carried out using the two most intense emission wavelengths of Ag at 328.068 nm and 338.289 nm. The total Ag

amounts in each sample were then determined through interpolation, from the calibration curve, in the Origin 8 pro software.[2]

Cytoviva Hyperspectral Microscopy of core AgNPs and ultrafiltered C@AgNPs

Small aliquots (~5 µL) of core AgNPs and ultrafiltered C@AgNPs were carefully deposited onto a glass microscope slide, covered with a glass microscope slip, and sealed with clear nail polish. The glass slides were allowed to dry for 2 hours and imaged in a CytoViva enhanced darkfield microscope (Olympus BX53) equipped with a 50 W halogen light source. A VNIR spectrophotometer (400-1000 nm) was utilized to perform sample imaging (10x Air objective, 60x, and 100x oil immersion objectives). A full scan of 696 lines (696 x 696 pixels) was employed using 60x and 100x oil immersion objectives and exposure times of 0.25-1.0 s. The ENVI 4.8 software was employed for the collection of hyperspectral data.[38]

Results and Discussion

Synthesis of core AgNPs and C@AgNPs

Silver nanoparticles were synthesized through the reduction of Ag^+ from $AgNO_3$ with $NaBH_4$.[37] This Creighton silver colloid is moderately dispersed in size and consists of mostly small AgNPs of an average diameter of ~10 nm (denoted core AgNPs).[40] The synthesis was carried out in excess $NaBH_4$ and ice-cold HQ water (Figure 5). The formation of core AgNPs was signaled by a change in color from colorless to a stable light yellow (Figure 6a). The basic reaction for the formation of core AgNPs is described in equation (1).[41]

$$AgNO_3 + NaBH_{4(excess)} + 4H_2O \longrightarrow Ag^0 + NaNO_3 + B(OH)_3 + 4H_2 + NaOH \qquad (1)$$

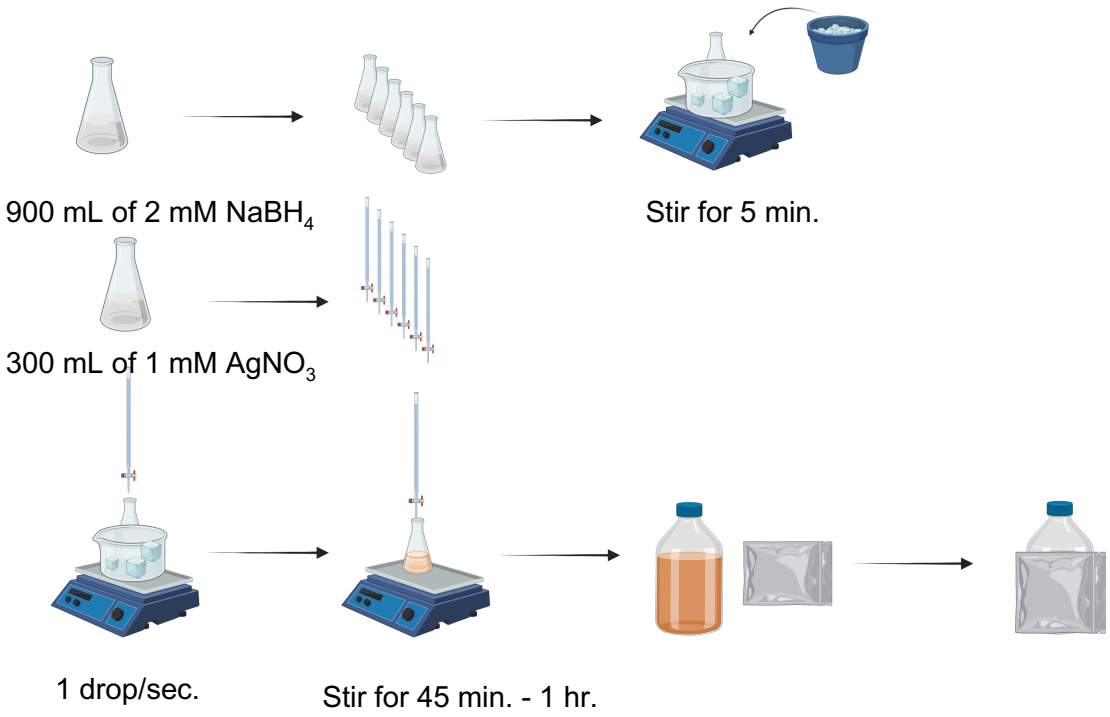

Figure 5. Step by step procedure for the synthesis of silver nanoparticles (AgNPs) via the modified Creighton method (made in ©BioRender - biorender.com).

Chlorothymol, the thymol derivative, was then utilized in the functionalization process of the core AgNPs. To the best of our knowledge, this is the first-time functionalization of Creighton core AgNPs with chorothymol (denoted C@AgNPs) was successfully explored. The colloidal C@AgNPs appeared muddy brown (Figure 6b) and were dispersed through ultrasonication. Ultrasonication was reported to decrease agglomeration and stimulate chemical reactions through collisions.[42] It also promotes the

formation of monodisperse organic hybrid materials containing NPs due to the resulting ultra-high surface area.[42] In this study, the use of ultrasonication led to a colloid that was stable for longer time periods (> 45 days, 4°C) when compared to the non-ultrasonicated C@AgNPs, which had a shelf life-time of about two weeks, at 4°C.[38] The stability of the colloidal C@AgNPs was confirmed via UV-Vis absorption measurements over the course of 45 days (Figure 7b). The ultrasonicated C@AgNPs were then ultrafiltered and ultracentrifuged as described in the Materials and Methods section for purification and separation from unbound chlorothymol molecules.

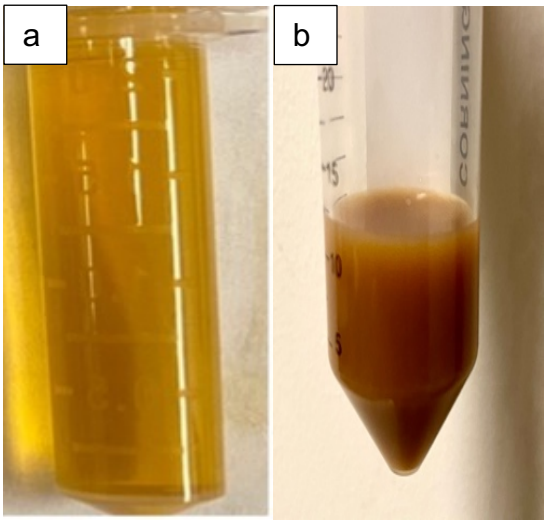

Figure 6. Physical appearance of: (a) core AgNPs (light yellow color) and (b) core AgNPs functionalized with chlorothymol, C@AgNPs (muddy brown color).

Characterization of core AgNPs and C@AgNPs

UV-Vis Absorption Spectrophotometry - The formation of core AgNPs was confirmed by the appearance of a surface plasmon resonance peak (SPR) at 400 nm. Functionalization of AgNPs with chlorothymol resulted in a shift of this SPR peak to 414 nm for the ultrafiltered C@AgNPs and 440 nm for the ultracentrifuged C@AgNPs at one day after synthesis (Figure 7a). The UV-Vis absorption spectrum of chlorothymol alone is provided in Figure 8. No absorption maxima were observed in the visible portion of the spectrum for chlorothymol control, further confirming the nanosurface modification with chlorothymol through the SPR peak shift. The very large SPR shift (from 400 nm to 440 nm) and the significant changes in the spectral profile of the ultracentrifuged C@AgNPs suggested the aggregation and subsequent increase in polydispersity of C@AgNPs through ultracentrifugation. Thus, ultrafiltration was deemed as being more efficient than ultracentrifugation in the size-selection and isolation of C@AgNPs with minimal aggregation. As a result, ultrafiltration was selected for the purification and isolation of C@AgNPs.

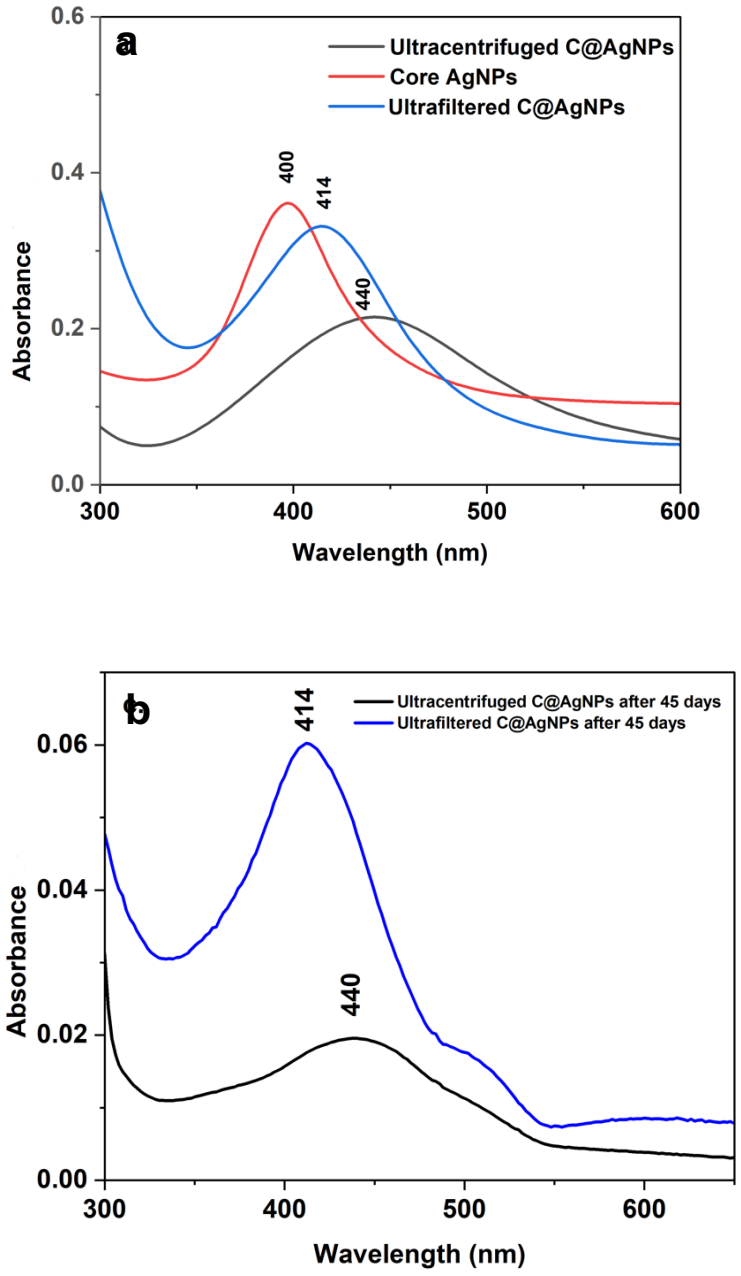

Figure 7. UV-Vis absorption spectra of (a) core AgNPs, ultrafiltered, and ultracentrifuged C@AgNPs one day after synthesis, and (b) 45 days after their manipulation by ultracentrifugation and ultrafiltration.

Both the ultracentrifuged and ultrafiltered C@AgNPs exhibited relatively good time stability. While no significant spectral changes were observed in the position of the SPR peaks over 45-days, there were significant increases in the full width at half maximum (FWHM) of the SPR peaks (Figure 7b). The FWHM of the SPR peak is a measure of the polydispersity in AgNPs and their aggregation state, where a large FWHM value is indicative of high polydispersity. [2, 6, 37] The FWHM values of the core and functionalized AgNPs were obtained using the gaussian fit function of the Origin 8.0 software. These FWHM values were provided in Table 1 at day 1 and day 45 after the synthesis. The FWHM value for the core AgNPs was estimated to be 63 nm at one day after synthesis. Upon functionalization with chlorothymol, the FWHM of ultrafiltered C@AgNPs increased to 64 nm, while the FWHM of ultracentrifuged AgNPs was 132 nm. The significant broadening in the SPR peak of ultracentrifuged C@AgNPs suggested the formation of larger C@AgNPs and C@AgNP-aggregates. After 45 days both the ultrafiltered and ultracentrifuged C@AgNPs exhibited an increase in their FWHM values to 73 nm and 143 nm, respectively, due to additional aggregation.

Table 1. Surface plasmon resonance (SPR) maxima and full width at half maximum (FWHM) values for the core AgNPs, ultrafiltered C@AgNPs, and ultracentrifuged C@AgNPs at day one and day 45 after synthesis.

Sample	SPR (nm)	FWHM (nm) after one day	FWHM (nm) after 45 days
Core AgNPs	**400**	**63**	**Not measured**
Ultracentrifuged C@AgNPs	**440**	**132**	**143**
Ultrafiltered C@AgNPs	**414**	**64**	**73**

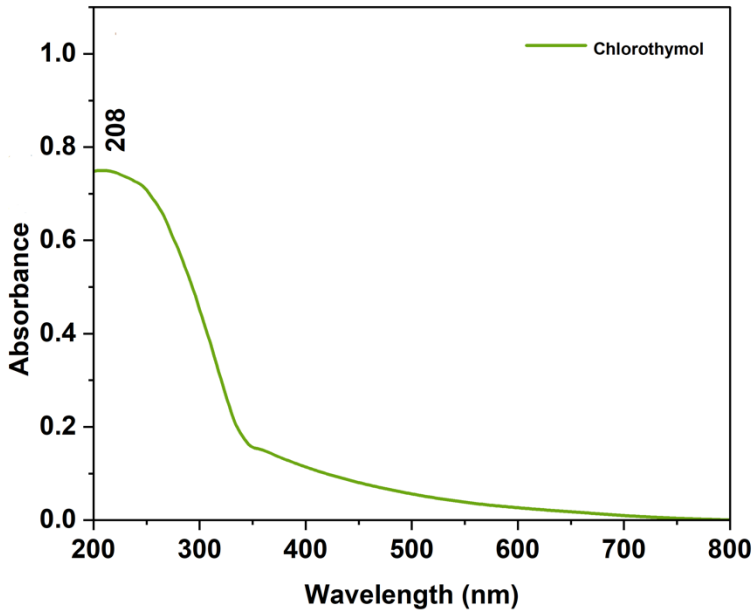

Figure 8. UV-Vis absorption spectrum of chlorothymol control.

Inductively coupled plasma-optical emission spectroscopy (ICP-OES) of core AgNPs and ultrafiltered C@AgnPs

The total amount of silver present in the core AgNPs and ultrafiltered C@AgNPs was determined by ICP-OES in conjunction with an external calibration curve through interpolation (Figure 9a). The concentration of silver in core AgNPs was 353.9 mg L^{-1} and significantly decreased to 72.16 mg L^{-1} in the ultrafiltered C@AgNPs (Figure 9b). The loss of silver might have occurred due to the compromised 10 kD filter used during the ultrafiltration procedure. It should be noted that a new filter could not be obtained due to the limited production during the COVID-19 pandemic. However, ultrafiltration is known to size-select and purify colloidal suspensions of AgNPs. As demonstrated in our previous work, most solvent, excess reagents and byproducts (e.g., free chlorothymol, sodium borohydride, ethanol, and water molecules) are collected together with the ultrafiltration permeate [39, 43] while the ultrafiltrate retentate contains purified C@AgNPs suspended in a small volume of solvent.

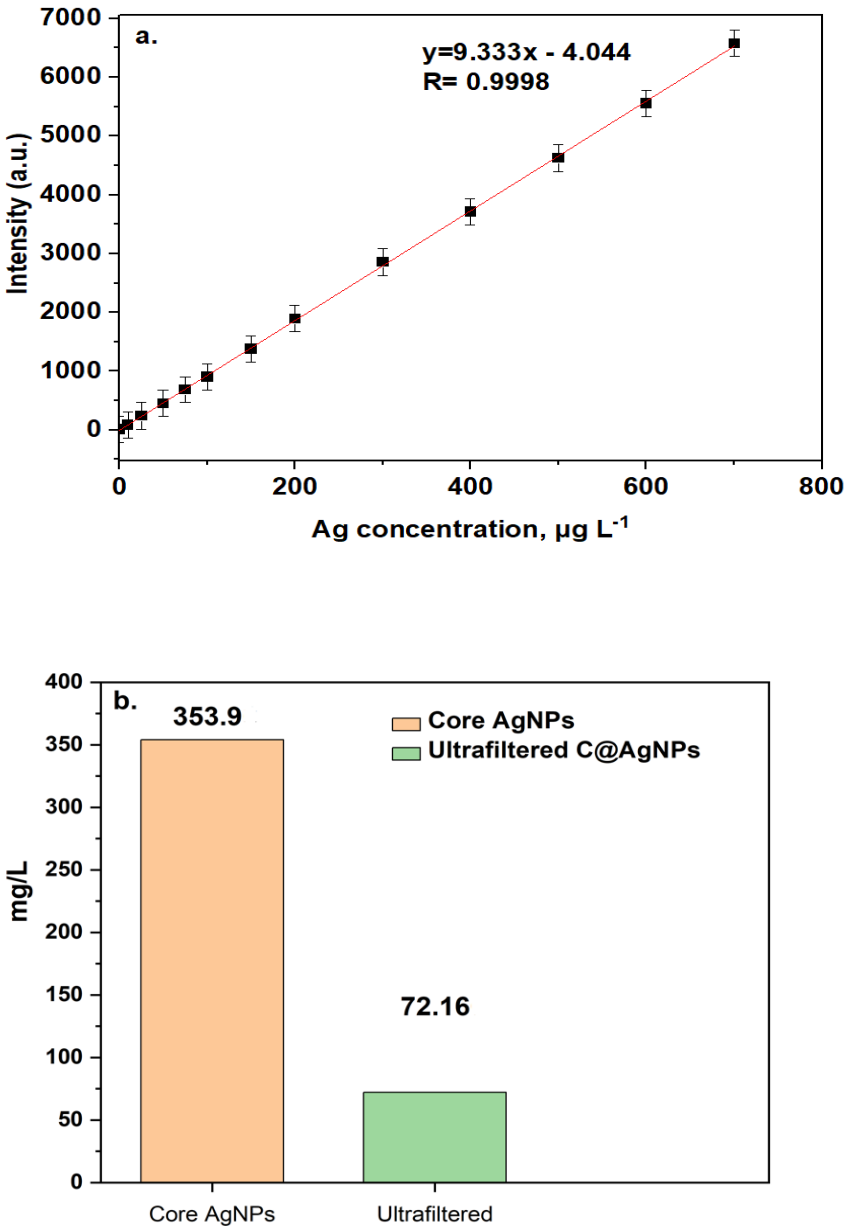

Figure 9. (a) ICP-OES external calibration curve for silver constructed with 13 standards, in the 0-700 µg L^{-1} concentration range. (b) Total silver amount in core AgNPs and ultrafiltered C@AgNPs.

Cytoviva Hyperspectral Microscopy of core AgNPs and ultrafiltered C@AgNPs

The CytoViva enhanced darkfield imaging (Figure 10) provided the hyperspectral signatures of core AgNPs (Figure 11) and ultrafiltered C@AgNPs (Figure 12). The scattering signature color coded in blue was associated with AgNPs of smaller size, while the scattering signal marked in red was attributed to larger AgNPs (Figures 11 and 12). The change in the light scattering was due to the change in the size of the NPs being studied. The analysis of 1800 pixels in the CytoViva image of core AgNPs showed that ~80% of the pixels were color coded in blue (455 nm), ~15% in green (586 nm), and ~5% in red (643 nm). The examination of 250 pixels in the CytoViva image of the ultrafiltered C@AgNPs showed that ~25% of the pixels were color coded in blue (465 nm), ~60% in green (615 nm), and ~15% in red (654 nm). One can notice a significant change in the size distribution of AgNPs upon functionalization with chlorothymol. While the percent contribution of blue AgNPs (small size) decreased by 55%, the percent contribution of green and red AgNPs (large sizes) increased by 45% and 10% respectively. Future transmission electron microscopy (TEM) studies are recommended for the confirmation of these results and the accurate estimation of these AgNP size ranges.

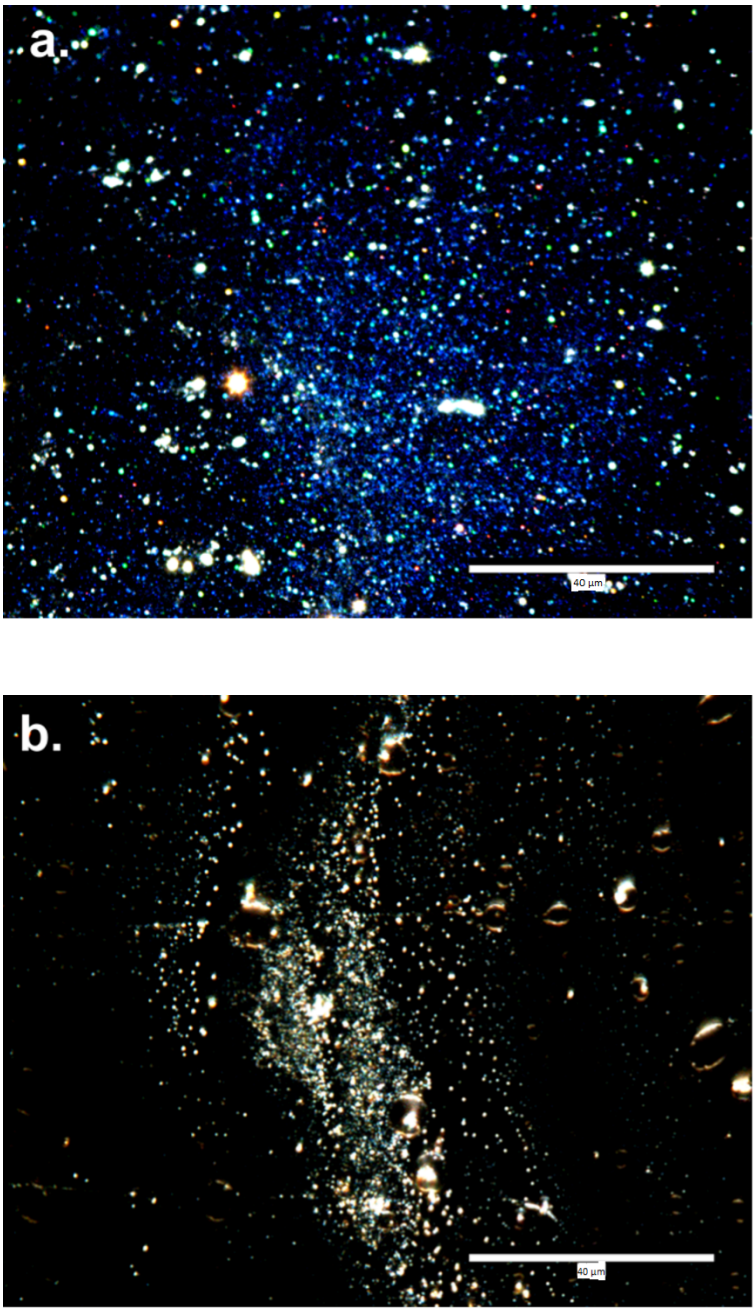

Figure 10. Cytoviva darkfield images of: (a) core AgNPs and (b) ultrafiltered C@AgNPs. Scale bar is 40 μm.

The hyperspectral features were also different for the core and C@AgNPs (Figures 11 and 12). For instance, the peak position and full width at half maximum (FWHM) values of the core AgNPs color coded in blue were smaller than those of the C@AgNPs functionalized with chlorothymol. The peak position for the blue core AgNPs was observed at 455 nm, with a FWHM of 35 nm (Table 2). On the other side, the ultrafiltered C@AgNPs color coded in blue experienced a red shift in peak position to 465 nm and an increase in the FWHM value to 50 nm (Table 3). Similar hyperspectral trends were observed for the ultrafiltered C@AgNPs color coded in green (615 nm) and red (654 nm). For instance, the FWHM value of the ultrafiltered C@AgNPs color coded in green was 55 nm, a larger value compared to 40 nm for the core AgNPs (Tables 2 and 3). Clearly, these changes in the signature features (peak position and FWHM) of the AgNPs of blue, green, and red color indicate an interaction between chlorothymol and AgNPs, and further confirm the nanosurface functionalization.

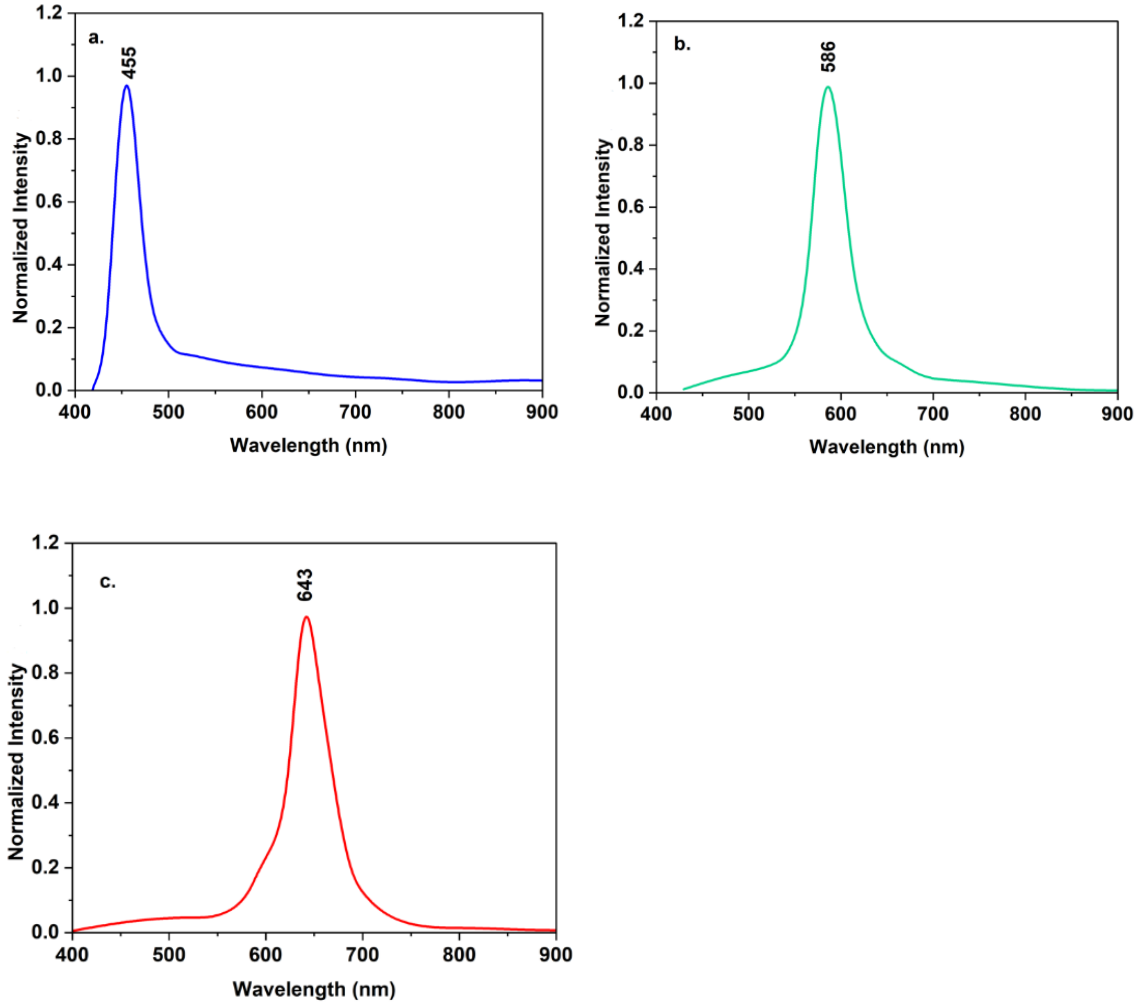

Figure 11. Average (N =20) Cytoviva hyperspectral signatures of core AgNPs color coded in (a) blue (455 nm), (b) green (586 nm), and (c) red (643 nm).

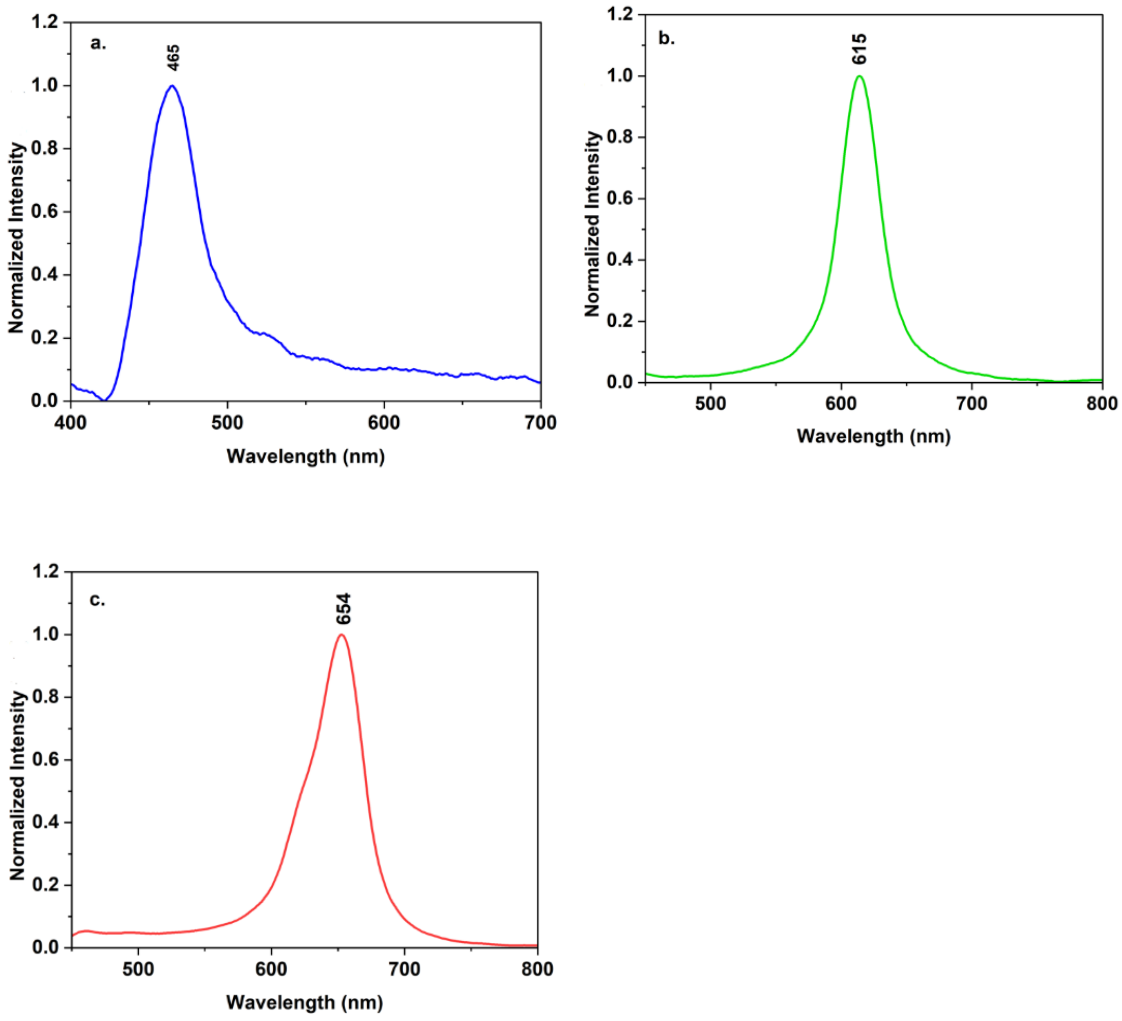

Figure 12. Average (N = 20) Cytoviva hyperspectral signatures of ultrafiltered C@ AgNPs color coded in (a) blue (465 nm), (b) green (615 nm), and (c) red (654 nm).

Table 2. Surface plasmon resonance maxima (SPR) and full width at half maximum (FWHM) values for the core silver nanoparticles (AgNPs).

AgNP sample	SPR (nm)	FWHM (nm)
Blue	**455**	**35**
Green	**586**	**40**
Red	**643**	**50**

Table 3. Surface plasmon resonance (SPR) peak position and full width at half maximum (FWHM) of the ultrafiltered, functionalized C@AgNPs color coded in blue, green, and red.

Ultrafiltered C@AgNP sample	SPR (nm)	FWHM (nm)
Blue	**465**	**50**
Green	**615**	**55**
Red	**654**	**60**

Raman Spectroscopy

The interaction of the OH^- group of thymol with AgNPs has been previously confirmed via Fourier Transform Infrared Spectroscopy (FT-IR).[10] Thus, the purity and the surface modification of the colloidal AgNPs to C@AgNPs color was confirmed in this study with the help of a complementary molecular spectroscopy method, *i.e.*, Raman spectroscopy. To achieve this, control Raman spectra of core AgNPs (no chlorothymol), 20% aqueous solution of ethanol, and chlorothymol solution controls were collected, assigned, and utilized in the analysis of the Raman spectrum of functionalized C@AgNPs color.

Core AgNPs exhibited only the characteristic peaks for water at ~1670 cm^{-1}, ~3263 cm^{-1}, and ~3397 cm^{-1}, which confirmed the purity of colloidal suspension.

The peak at ~1670 cm^{-1} occurred as the result of H-O-H bending mode, the peak at ~3263 cm^{-1} corresponded to the symmetric OH stretching, and the peak at 3397 cm^{-1} was due to the asymmetric OH stretching (Figure 13). [2]

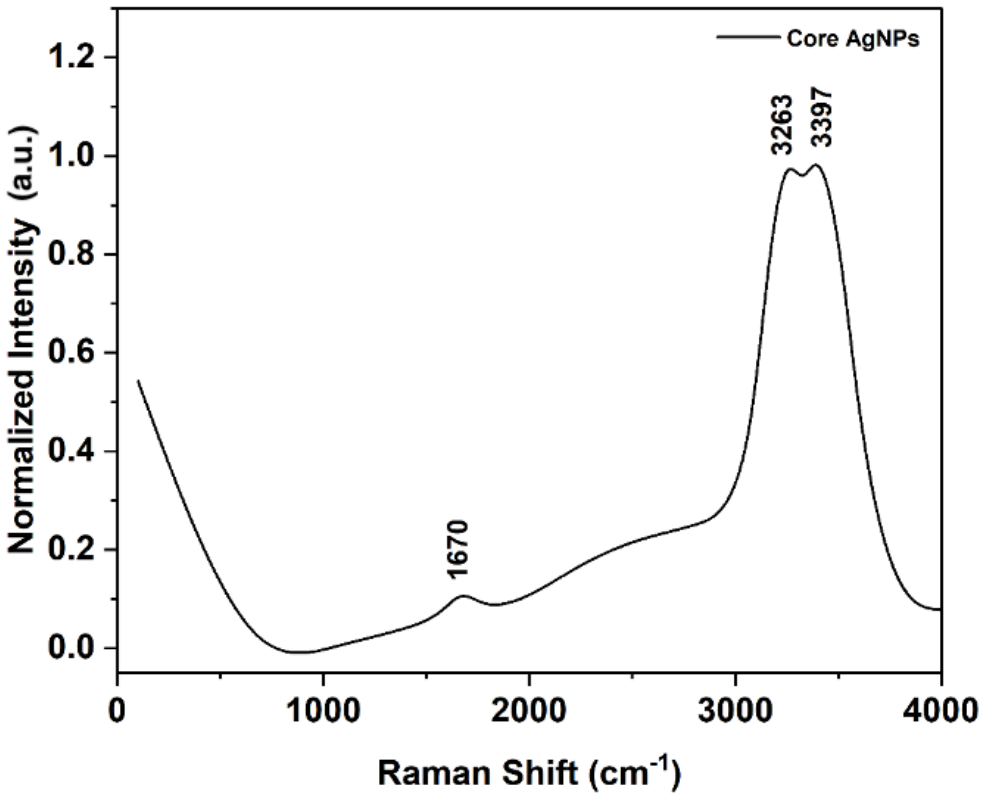

Figure 13. Raman spectrum of core AgNPs suspended in water.

The chlorothymol solution was prepared by dissolving it in 20 % aqueous ethanol and its Raman spectrum was collected (Figure 14). The fingerprint peaks of ethanol were assigned as follows: 440 cm^{-1} to the C-O stretching, 879 cm^{-1} to the C-C-O stretching, 1045 and 1049 cm^{-1} to the C-C stretching, 1286 cm^{-1} to the CH_2 twisting vibration, 1458 cm^{-1} to the asymmetric vibration in CH_3 group, 2890 and 2936 cm^{-1} to the symmetric and asymmetric stretching of C-H in CH_3 group, respectively.[44]

The peaks at 1643, 3246, and 3382 cm^{-1} were attributed to the same OH vibrational modes of water present.[2]

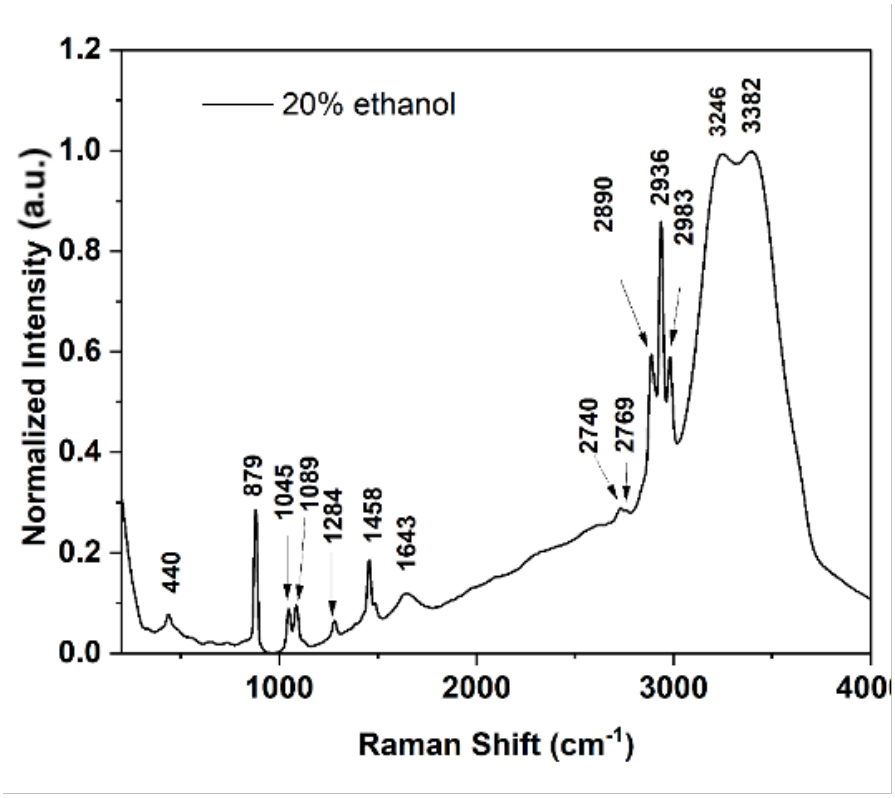

Figure 14. Raman spectrum of control 20% aqueous ethanol solution.

The Raman spectrum of the chlorothymol in 20% aqueous ethanol solution is shown in Figure 15. The peak at ~3286 cm^{-1} represents the O-H stretching vibration mode of the phenol group. Stretching vibration modes for the C-H bond in alkanes occurred in the 2840-3000 cm^{-1} spectral range. The peaks characteristic to the isopropyl groups appeared at lower frequencies, namely 2714 and 2750 cm^{-1} due to the presence of the Cl atom in the structure of chlorothymol (Figure 2). The C=C stretching of the benzene ring occurred near 1579 and 1620 cm^{-1}, while the bending vibration modes of the

CH_3 in isopropyl group appeared as a doublet of almost equal intensities near 1381 cm^{-1} (symmetrical) and 1460 (asymmetrical) cm^{-1}.

The peak at 1275 cm^{-1} was assigned to the C-O stretching vibration mode. In-plane and out-of-plane bending of the C-H groups of the aromatic ring were observed at 1102 and 1070 cm^{-1} bands, respectively. Bands at 728 and 757 cm^{-1} were associated with the C-O and -OH out of plane bending vibration modes, respectively. The peak at ~1070 cm^{-1} may be the result of the C-Cl bending vibration mode. The other Raman bands between 171-435 cm^{-1} were attributed to the vibrational modes of the aromatic ring. [45] A more detailed tentative assignment of the observed Raman peaks is shown in Table 4.

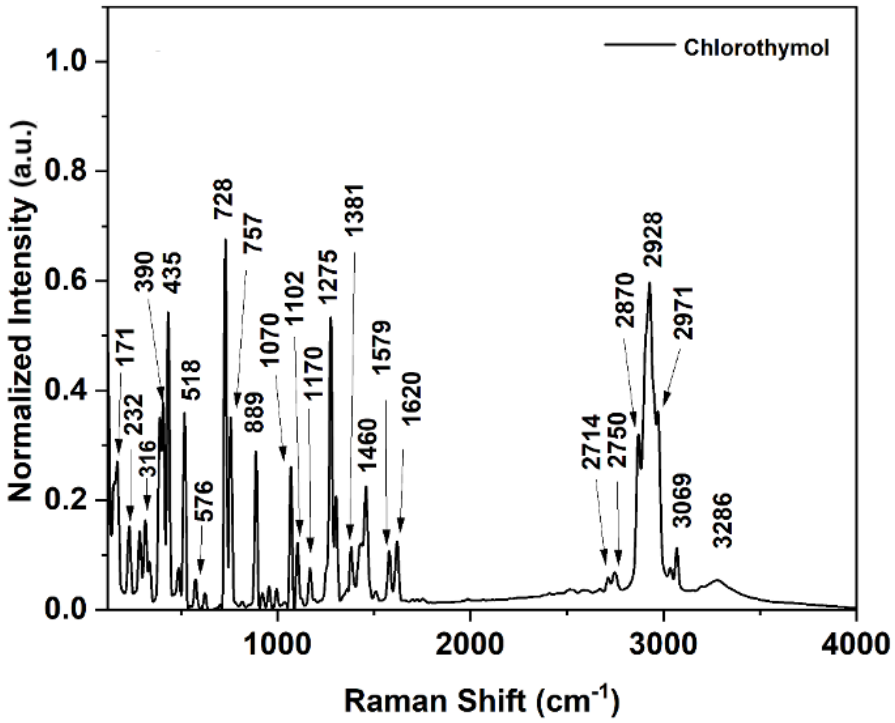

Figure 15. Raman spectrum of chlorothymol control in 20% aqueous ethanol solution.

Table 4. Experimental Raman peaks of the chlorothymol solution and their tentative spectral assignments according to the literature.

Observed Raman Peaks (cm^{-1})	**Tentative assignment**
728	C-O out of plane bending [42, 45]
757	OH out of plane bending [42, 47]
889	Out of plane rocking CH_3 of isopropyl group [46]
1070	C-Cl bending [48]
1102	Out of plane C-H vibration [46]
1275	C-O stretching [46]
1381	Bending of CH_3 in the isopropyl group [46]
1460	Bending of CH_3 in the isopropyl group [46]
1579	C=C stretching of the benzene ring [46]
1620	C=C stretching of the benzene ring [46]

The Raman spectra of the AgNPs functionalized with chlorothymol (C@AgNPs) shown in Figure 16 exhibited the water characteristic peaks at ~1635 cm^{-1} (OH bending vibration mode), ~3238 cm^{-1} (OH symmetric stretching), and ~3414 cm^{-1} (asymmetric stretching).[2] In addition, several of

the Raman peaks characteristic to chlorothymol were observed by comparison to the core AgNPs control. This is indicative of the surface functionalization of core AgNPs with chlorothymol. More specifically, the Raman bands at 1354 cm^{-1} and 1470 cm^{-1} of lower intensity were associated with the CH_3 moieties of the isopropyl group in chlorothymol.[45] The peak at ~1093 cm^{-1} was most likely the result of the shift in the C-Cl stretching mode of chlorothymol upon functionalization.[46] The weak bands at ~2050 cm^{-1} and ~2385 cm^{-1} were attributed to the C=C bonds of the aromatic ring in chlorothymol.[45] The band at 718 cm^{-1} was assigned to the C-O out-of-plane bending vibration mode of chlorothymol. The OH out-of-plane bending vibration mode at ~757 cm^{-1} characteristic to chlorothymol was not present in the spectrum of C@AgNPs suggesting a potential interaction between the O atom of chlorothymol and the Ag atoms of the nanosurface.[45]

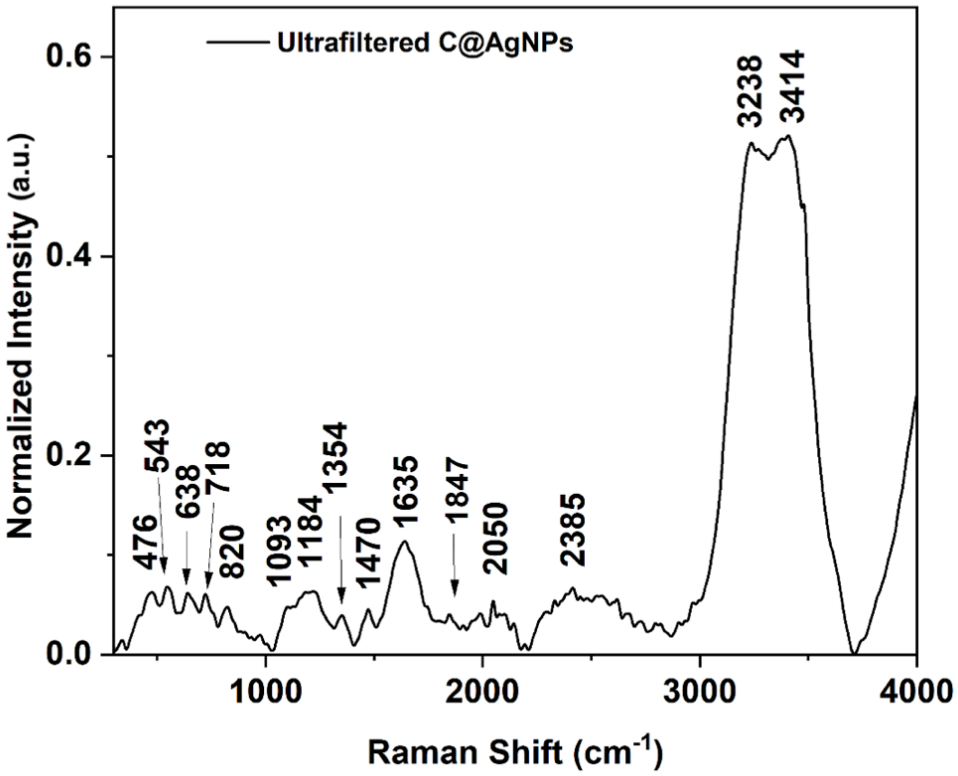

Figure 16. Raman spectrum of ultrafiltered C@AgNPs.

In addition, a broad peak appeared between 1100 and 1300 cm^{-1} in the Raman spectrum of C@AgNPs. Its deconvolution confirmed the presence of the C-O stretching mode of chlorothymol at ~1270 cm^{-1} (Figure 17). The deconvolution process was performed using a Gaussian fit, in the Origin software, with the help of the multiple peak fit function and the following parameters were selected: y_0-representing the base of the peak, xc-center, A-amplitude, and w-FWHM. The peak centers were utilized for the deconvolution fitting.

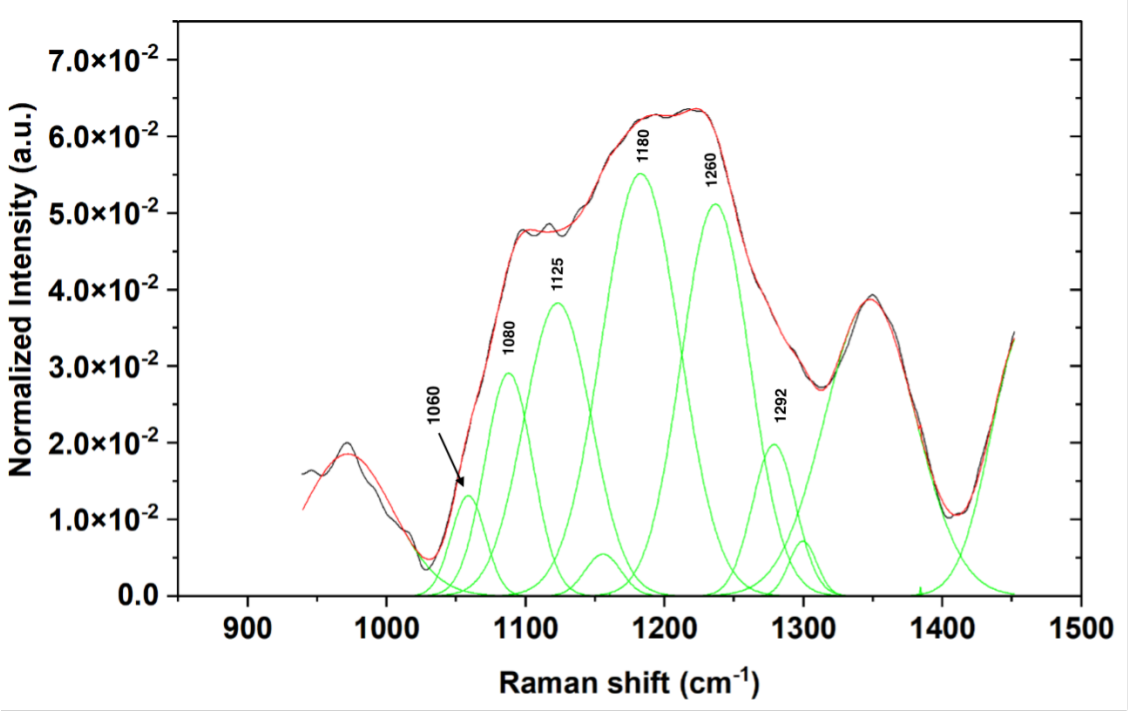

Figure 17. Deconvolution of the Raman spectrum of C@AgNPs using a Gaussian fi

SEM and XRD analysis

Figure 18 shows a representative SEM image of the ultrafiltered C@AgNPs and the corresponding EDX spectrum.

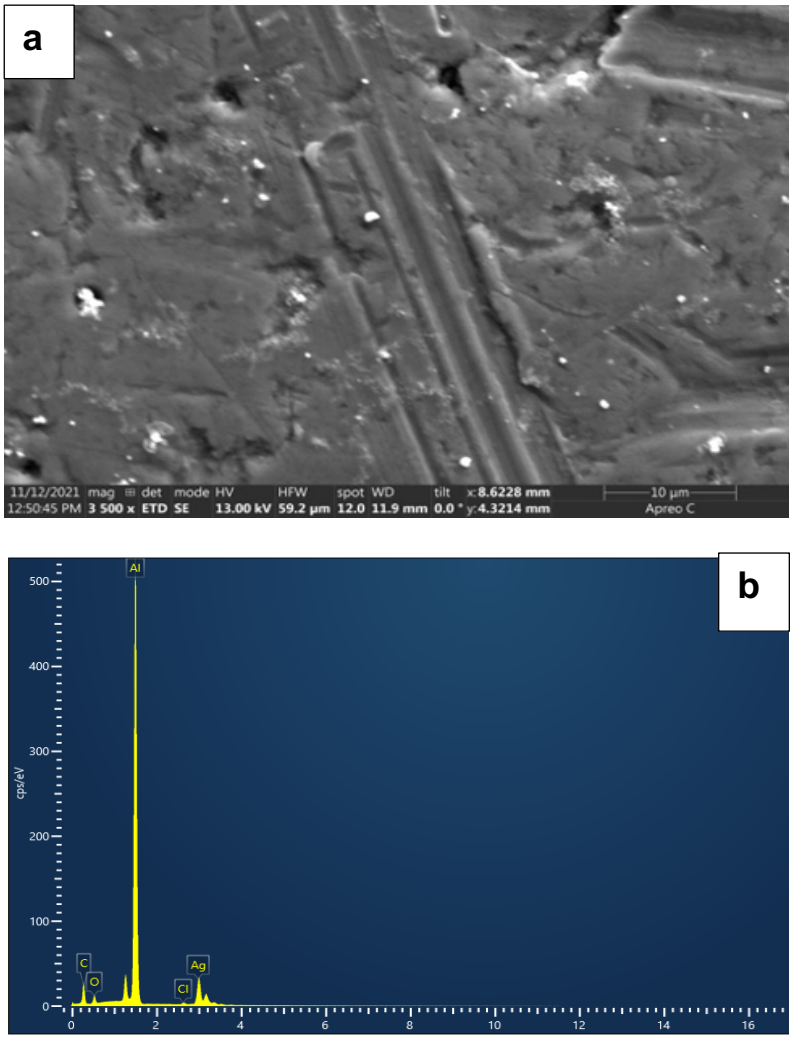

Figure 18. (a) SEM image of the ultrafiltered C@AgNPs (scale bar-10 µm) and (b) the corresponding EDX spectrum.

No conclusion could be drawn at this time with respect to the size of functionalized C@AgNPs because of the small resolution (scale bar 10 μm). Future SEM images should be collected with higher resolution to overcome this limitation. The peak at 0.25 keV corresponded to C_{KA}, while the other two peaks at 0.55 keV and 3 keV were due to O_{KA} and Ag_{La}. The peak at 2.6 keV was assigned to Cl_K. [49] The aluminum peak at 1.5 keV was attributed to the aluminum stem stub used to hold the samples.

The presence of C, O, and Cl peaks in the EDX spectrum is an indication of the functionalization of core AgNPs with chlorothymol. Table 5 includes the weight (wt.) % of the elements in the ultrafiltered C@AgNPs containing organic components, C, O (21.16 %and 3.60%) and Cl (0.20 %) corresponding to chlorothymol. The Al present (54.13 %) comes from the mount stem stub. The percentage of Ag showed to be 22.35 %. The percentages deducted from the EDX spectrum represent the concentration of each element in the sample. Future efforts should be dedicated to correlating the element percentages to the loading efficacy of chlorothymol in AgNPs.

Table 5. Percentage weight of elements present in the ultrafiltered C@AgNPs revealed by the EDX analysis.

Element	Wt. %
C	**21.16**
O	**3.60**
Al	**54.13**
Ag	**22.35**
Cl	**0.20**

Proposed mechanism of functionalization of AgNPs with chlorothymol

Silver is a transition metal located in group 11 (IB) and period 5 of the periodic table. Thus, silver with an electronic configuration of [Kr] $4d^{10}5s^{1}$ has empty $5p^{0}$ and $5d^{0}$ orbitals available for chemical interactions. In the chlorothymol molecule, both chlorine and oxygen have free electron pairs to donate and form a coordinate-covalent bond with Ag atom.

Oxygen atom has greater electron-donor power than chlorine. Thus, oxygen may donate its electron pairs to the free vacant orbital of the Ag atom resulting in a coordinate-covalent bond between the O and Ag atom as it was suggested by the Raman data. More specifically, the possible interaction between Ag and O upon C@AgNP functionalization is supported by the absence of the characteristic Raman OH peak of chlorothymol at 757 cm^{-1} (Figure 16).[45]

Upon AgNPs functionalization with chlorothymol cations in solution, an electrostatic, positive shield is formed around the AgNPs. As a result, C@AgNPs repulse each other electrostatically and separate in the colloidal suspension, offering long term stability for the colloidal product and potential future applications (Figure 19).

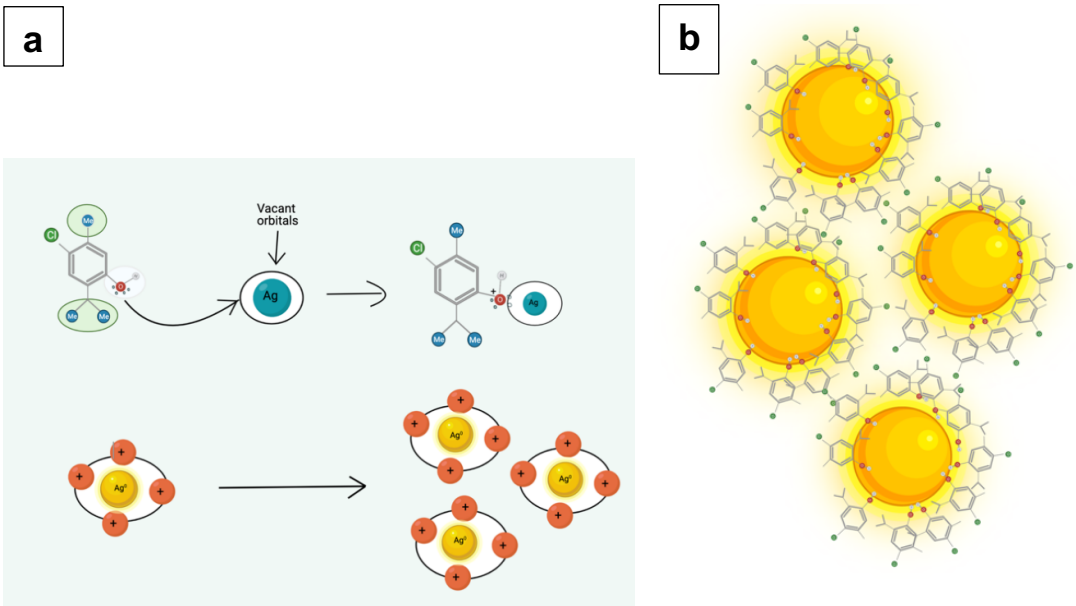

Figure 19. Schematic representation of (a) the formation of the coordinate-covalent bond between Ag^0 and free electron pairs of the O atom in the chlorothymol molecules and (b) the stabilization mechanism of the C@AgNPs via electrostatic repulsions (made in ©BioRender -biorender.com).

Conclusions

This study aimed to modify the surface of core silver nanoparticles (AgNPs) with an antibacterial agent, chlorothymol, via a covalent conjugation between O and Ag. Equal volumes of AgNPs suspension and chlorothymol solutions in 20% ethanol were mixed and sonicated for 2 hours, at 35 °C. A change in color from yellow to muddy brown was observed, suggesting the formation of functionalized AgNPs. The physicochemical properties of the core AgNPs and the novel AgNPs functionalized with chlorothymol (C@AgNPs) were characterized by UV-Vis absorption spectroscopy, Raman spectroscopy, ICP-OES, Cytoviva hyperspectral imaging, and SEM/EDX analysis. These measurements confirmed the functionalization of core AgNPs with chlorothymol and the proposed mechanism of formation for the C@AgNPs through a coordinated covalent bond between the oxygen atom of chlorothymol and the Ag atoms at the nano surface.

Future work needs to be focused on studying the loading efficacy of chlorothymol in AgNPs by thermogravimetric analysis (TGA), the size distribution by TEM, the AgNP surface charge by Zeta potential measurements, as well as on testing the antibacterial properties C@AgNPs. In addition, the biocompatibility of the novel C@AgNPs and possible use for wound healing is something worth exploring.

References

(1) Prabhu, S.; Poulose, E. K. Silver Nanoparticles: Mechanism of Antimicrobial Action, Synthesis, Medical Applications, and Toxicity Effects. *Int. Nano Lett.* **2012**, 2 (1), 32. https://doi.org/10.1186/2228-5326-2-32

(2) Wilcox, A. M. Silver Nanoparticles: An Effective Antibacterial Agent Against Gram-Negative Bacteria. MS Theis, *Wright State University*, **2019**. https://corescholar.libraries.wright.edu/etd_all/2264/

(3) Slavin, Y. N.; Asnis, J.; Häfeli, U. O.; Bach, H., Metal nanoparticles: understanding the mechanisms behind antibacterial activity. J. *Nanobiotechnology.* **2017**, *15* (1), 65.

(4) Mikhailova, E.O. Silver Nanoparticles: Mechanism of Action and Probable Bio-Application. *J. Funct. Biomater.* **2020**, 11 (4), 84. https://doi.org/10.3390/jfb11040084

(5) Rajeshkumar, S.; Bharath, L.V. Mechanism of plant-mediated synthesis of silver nanoparticles – A review on biomolecules involved, characterization and antibacterial activity, *Chem. Biol. Interact .***2017**, 273, 219-227. https://doi.org/10.1016/j.cbi.2017.06.019

(6) Agnihotri, S.; Mukherji, S.; Mukherji. S. Size-Controlled Silver Nanoparticles Synthesized Over the Range 5-100 nm Using the Same Protocol and Their Antibacterial Efficacy. *RSC Adv.* **2014**, 4 (8), 3974–3983. https://doi.org/10.1039/c3ra44507k

(7) Auffan, M., Rose, J., Bottero, J.-Y., Lowry, G. V., Jolivet, J.-P., and Wiesner, M. R. Towards a Definition of Inorganic Nanoparticles from an Environmental, Health and Safety Perspective. *Nat. Nanotechnol.* **2009**, 4 (10), 634–641. https://doi.org/10.1038/nnano.2009.242

(8) Lok, C. N.; Ho, C. M.; Chen, R.; He, Q. Y.; Yu, W. Y.; Sun, H.; Tam, P. K. H.; Chiu, J. F.; Che, C. M. Proteomic Analysis of the Mode of Antibacterial Action of Silver Nanoparticles. J. *Proteome Res*. **2006**, 5 (4), 916–924. https://doi.org/10.1021/pr0504079

(9) Thiruppathi, R.; Mishra, S.; Ganapathy, M.; Padmanabhan, P.; Gulyás, B. Nanoparticle Functionalization and its Potentials for Molecular Imaging. *Adv. Sci*. **2017**, 4, 1600279. https://doi.org/10.1002/advs.201600279

(10) Manukumar, H. M.; Umesha, S.; Kumar, H. N. N. Promising Biocidal Activity of Thymol Loaded Chitosan Silver Nanoparticles (T-C@AgNPs) as Anti-Infective Agents Against Perilous Pathogens. *Int. J. of Biol. Macromol.* **2017**, 102, 1257–1265. https://doi.org/10.1016/j.ijbiomac.2017.05.030

(11) Cheung, R. C. F.; Ng, T. B.; Wong, J. H.; Chan, W. Y. Chitosan: An Update on Potential Biomedical and Pharmaceutical Applications. Mar. Drugs. 2015, 13 (8), 5156–5186. https://doi.org/10.3390/md13085156

(12) Wattanasatcha, A.; Rengpipat, S.; Wanichwecharungruang, S. Thymol Nanospheres as an Effective Anti-Bacterial Agent. *Int. J. Pharm.* **2012**, 434 (1-2), 360–365. https://doi.org/10.1016/j.ijpharm.2012.06.017

(13) Memar, M. Y.; Raei, P.; Alizadeh, N.; Aghdam, M. A.; Kafil, H. S. Carvacrol and Thymol: Strong Antimicrobial Agents against Resistant Isolates. *Rev. Med. Microbiol*. **2017**, 2, 63-68. https://doi.org/10.1097/MRM.0000000000000100

(14) Environmental Protection Agency (EPA). [Rule]. Thymol; Exemption from the Requirement of a Tolerance. 71 FR 2889. Effective Date: 08.18.2006. https://www.federalregister.gov/documents/2006/01/18/06-436/thymol-exemption-from-the-requirement-of-a-tolerance (accessed 2021).

(15) Food and Drug Administration (FDA). Department of Health and Human Services. Chapter 1: Title 21- Food and Drugs. Subchapter D-Drugs for Human Consumption. Part 170-Food Additives, Subpart E-Generally Recognized as Safe (GRAS) Notice. 21CFR170.203. (Last updated Jan. 06, 2022).

(16) Kaur, R.; Darokar, M. P.; Chattopadhyay, S. K.; Krishna, V.; Ahmad, A. Synthesis of Halogenated Derivatives of Thymol and Their Antimicrobial Activities. *Med. Chem. Res*. **2014**, 23 (5), 2212–2217. https://doi.org/10.1007/s00044-013-0809-8

(17) Jones, A., Barker Haliski, M., Ilie, A.S. et al. A Multiorganism-Pipeline for Antiseizure Drug Discovery: Identification of Chlorothymol as a Novel γ Aminobutyric Acidergic Anticonvulsant. *Epilepsia.* **2020**, 61 (10), 2106-2118. https://doi.org/10.1111/epi.16644

(18) Kumar, S.; Mina, P. R.; Kumar, R.; Pal, A.; Ahmad, A.; Tandon, S.; Darokar, M. P. 4-Chlorothymol Exerts Antiplasmodial Activity Impeding Redox Defense System in Plasmodium Falciparum. *Front. Pharmacol.* **2021**, 12, 628970 https://doi.org/10.3389/fphar.2021.628970

(19) Andersen, A. Final Report on the Safety Assessment of Sodium P-Chloro-m-Cresol, p-Chloro-m-Cresol, Chlorothymol, Mixed Cresols, m-Cresol, o-Cresol, p-Cresol, Isopropyl Cresols, Thymol, o-Cymen-5-ol, and Carvacrol. *Int. J. Toxicol.* **2006**, 25 (1), 29–127. https://doi.org/10.1080/10915810600716653

(20) Food and Drug Administration (FDA). Department of Health and Human Services. Title 21-Food and Drugs. Chapter 1. Subchapter D-Drugs for Human Use. Part 310-New Drugs. Subpart E, a (22). 21CFR210.545. https://www.accessdata.fda.gov/scripts/cdrh/cfdocs/cfcfr/cfrsearch.cfm (accessed 2021).

(21) Justin, T. UV-Vis Spectroscopy: Principle, Strengths, Limitations and Applications. Technology Networks (Sudbury, UK), June 30, 2021, updated December 16, 2021. https://www.technologynetworks.com/analysis/articles/uv-vis-spectroscopy-principle-strengths-and-limitations-and-applications-349865 (accessed 2-20-2022).

(22) Pockrand, I.; Swalen, J.D.; Gordon, J.G.; Philpott. M.R. Surface plasmon spectroscopy of organic monolayer assemblies, *Surf. Sci.* **1978**, 74 (1), 237-244. https://doi.org/10.1016/0039-6028(78)90283-2

(23) Wu, C., Zhou, X. & Wei, J. Localized Surface Plasmon Resonance of Silver Nanotriangles Synthesized by a Versatile Solution Reaction. *Nanoscale Res. Lett*. **2015**, 10, 354. https://doi.org/10.1186/s11671-015-1058-1

(24) Hou, W. and Cronin, S.B. A Review of Surface Plasmon Resonance-Enhanced Photocatalysis. *Adv. Funct. Mater.* **2013**, 23 (13), 1612- 1619. https://doi.org/10.1002/adfm.201202148

(25) nanoComposix. UV/VIS/NIR Spectroscopy Analysis of Nanoparticles. nanoComposix, **2012**. http://50.87.149.212/sites/default/files/nanoComposix%20Guidelines%20for%20UV-vis%20Analysis.pdf (accessed 11-25-2021).

(26) Owen, T. Fundamentals of Modern UV-visible spectroscopy. In Principles and Applications of UV-visible spectroscopy, primer.; *Agilent Technologies*, **2000**, pp 10-21.

(27) Olesik, J. W. Elemental Analysis Using ICP-OES and ICP/MS. *Anal. Chem.* **1991**, 63 (1), 12A–21A. https://doi.org/10.1021/ac00001a711

(28) Agilent. ICP-OES FAQ's including the ICP-OES Principle, ICP-OES Instrument, and ICP-OES Analysis. Agilent. https://www.agilent.com/en/support/atomic-spectroscopy/inductively-coupled-plasma-optical-emission-spectroscopy-icp-oes/icp-oes-instruments/icp-oes-faq (accessed 11-26-2021).

(29) Ravanshad, R.; Karimi Zadeh, A.; Amani, A. M.; Mousavi, S. M.; Hashemi, S. A.; Savar Dashtaki, A.; Mirzaei, E.; Zare, B. Application of Nanoparticles in Cancer Detection by Raman Scattering Based Techniques. *Nano Rev. Exp.* **2017**, 9 (1), 1373551. https://pubmed.ncbi.nlm.nih.gov/30410710/

(30) Gurvinder Sing Bumbrah; Rakesh Mohan Sharma. Raman Spectroscopy-Basic Principle, Instrumentation and Selected Applications for the Characterization of Drugs of Abuse. *Egypt J. Forensic Sci.* **2016**, 6 (3), 209–215. https://doi.org/10.1016/j.ejfs.2015.06.001

(31) Beattie, R. J.; McGarvey, J. J.; Stitt, W. A. Raman spectroscopy for the detection of AGEs/ALEs. *Methods mol. bio.* **2013**, 965. 297-312. https://doi.org/10.1007/978-1-62703-239-1_20

(32) Zamora-Perez, P.; Tsoutsi, D.; Xu, R.; Rivera-Gil, P. Hyperspectral-Enhanced Dark Field Microscopy for Single and Collective Nanoparticle Characterization in Biological Environments. Materials. **2018**, 11(2), 243. https://doi.org/10.3390/ma11020243

(33) Horiba. HORIBA and CytoViva: Combining Technologies for Smarter Nanoparticle Detection. Horiba. https://www.horiba.com/int/raman-edf-hsi/ (last accessed 2022)

(34) Mehta, N.; Shaik, Sh.; Rm, D.; Gartia, R. M. Single-Cell Analysis Using Hyperspectral Imaging Modalities. *J. Biomech. Eng.* **2018**, 140 (2), 0208021–02080216. https://doi.org/10.1115/1.4038638

(35) Zhang, X. F.; Liu, Z. G.; Shen, W.; Gurunathan, S. Silver Nanoparticles: Synthesis, Characterization, Properties, Applications, and Therapeutic Approaches. *Int. J. Mol. Sci.* **2016**, 17 (9), 1534. https://doi.org/10.3390/ijms17091534

(36) Swapp, S. Scanning Electron Microscopy (SEM). SERC, 2017. https://serc.carleton.edu/research_education/geochemsheets/techniques/SEM.html (accessed 01-20-2022).

(37) Paluri, S. L. Synthesis, Characterization and Manipulation of Creighton Silver Synthesis, Characterization and Manipulation of Creighton Silver Nanoparticles for Future Cytotoxicity Studies. MS Thesis, *Wright State University*, **2011**. https://corescholar.libraries.wright.edu/etd_all/536/

(38) Steingass, K. Cytoviva Hyperspectral Imaging for Comparing the Uptake and Transformation of AgNPs and Ag^{+} in Mitochondria. MS Thesis, *Wright State University*, **2021**. http://rave.ohiolink.edu/etdc/view?acc_num=wright1630267087380931

(39) Dorney, Kevin & Baker, Joshua & Edwards, Michelle & Kanel, Sushil & O'Malley, Matthew & Sizemore, Ioana. (2014). Tangential Flow Filtration of Colloidal Silver Nanoparticles: A "Green" Laboratory Experiment for Chemistry and Engineering Students. *J. Chem. Educ*. **2014**, 91 (7), 1044-1049. https://doi.org/10.1021/ed400686u

(40) Trefry, J. C.; Monahan, J. L.; Weaver, K. M.; Meyerhoefer, A. J.; Markopolous, M. M.; Arnold, Z. S.; Wooley, D. P.; Pavel, I. E. Size Selection and Concentration of Silver Nanoparticles by Tangential Flow Ultrafiltration for SERS-Based Biosensors. *J. Am. Chem. Soc*. **2010**, 132 (32), 10970–10972. https://doi.org/10.1021/ja103809c

(41) Pavel, I. E.; Alnajjar, K. S.; Monahan, J. L.; Stahler, A.; Hunter, N. E.; Kent, M.; Baker, J. D.; Meyerhoefer, A. J.; Dolson, D. A. Estimating the Analytical and Surface Enhancement Factors in SERS: A Novel Physical Chemistry and Nanotechnology Laboratory Experiment. *J. Chem. Educ*. **2012**, 89 (2), 286-290. https://doi.org.10.1021/ed200156n

(42) Bera, S.; Mondal, D. A Role for Ultrasound in the Fabrication of Carbohydrate-Supported Nanomaterials. *J. Ultrasound*. **2019**, 22, 131–156. https://doi.org/10.1007/s40477-019-00363-8

(43) Dorney, K. M. A Chemical Free Approach for Increasing the Biochemical Surface-Enhanced Raman Spectroscopy (SERS)-Based Sensing Capabilities of Colloidal Silver Nanoparticles. MS Thesis, *Wright State University*, **2014**. https://corescholar.libraries.wright.edu/etd_all/1199/

(44) Pappas, C.; Marianthi, B.; Konstantinou, E.; Proxenia, N.; Kallithraka, S.; Kotseridis, Y.; Taranilis, P. A. Evaluation of a Raman Spectroscopic Method for the Determination of Alcohol Content in Greek Spirit Tsipouro. *Curr. Res. Nutr. Food Sci.* **2016**, 4 (2), 1–9. https://doi.org/10.12944/CRNFSJ.4.Special-Issue-October.01

(45) Gupta, R. A Theoretical Study of 5-Methyl-2-Isopropylphenol (Thymol) by DFT. *Int. J. Sci. Res. Sci. Technol.* **2021**, 8 (3), 812–830. https://doi.org/10.32628/ijsrst2183182

(46) Lee, Moon-Kwon, Kim, Hye-Sung, Rhee, Hak-June. Reaction Monitoring of Imine Synthesis Using Raman Spectroscopy. Bull. Korean *Chem. Soc.* **2003**, 24 (2), 205–208. https://doi.org/10.5012/BKCS.2003.24.2.205

(47) Hoang, V.-T.; Mai, M.; Thi Tam, L.; Vu, N. P.; Tien Khi, N.; Dinh Tam, P.; Quang Huy, T.; Le, A.-T.; Xuan Dinh, N.; Tran, V.-H. Functionalized-AgNPs for Long-Term Stability, and its Applicability in the Detection of Manganese ions. *Adv. Polym. Technol.* **2020**, 2020, 1-9. https://doi.org/10.1155/2020/9437108

(48) Larkin, J. P. IR and Raman Spectra-Structure Correlations: Characteristic Group Frequencies. IR and Raman Spectroscopy: Principles and Spectral Interpretation, 1st. Ed.; Elsevier, **2011**, pp 76-100.

(49) Anders, C. B. A SERS and SEM-EDX Study of the Antiviral Mechanism of Creighton Silver Nanoparticles against Vaccinia Virus. MS Thesis, Wright State University, 2012. https://corescholar.libraries.wright.edu/etd_all/1089/